Development of finite-volume-based full-MHD code for internal and external MHD instabilities

Y. Kagei[1], Y. Kishimoto[2,1] T. Miyoshi[3] and M. Takechi[1]

[1] Fusion Research and Development Directorate, JAEA, Japan

[2] Grad. School of Energy Sci., Kyoto Univ., Japan

[3] Grad. School of Science, Hiroshima University, Japan

11th WORKSHOP ON MHD STABILITY CONTROL
Nov. 6-8, 2006
Princeton, NJ, USA

Introduction

- Finite volume method
  - Valid for the boundaries with an arbitrary geometry
  - Possible to naturally discretize the conservation law
  - Deal with MHD eq. by adding a magnetic source term to fluid eq.
  - Expected to improve the issue of divergence-free condition

- Development of a finite-volume-based full-MHD code, MHFVSP
  - Recent progress of MHFVSP code
    - Upgraded to deal with unstructured triangular elements
    - Implementation of the pseudo-vacuum model

- Nonlinear simulation study using MHFVSP code
  - Interactions among different scale modes and its role in the saturation mechanism

Compressible MHD equations

An electromagnetic source term and a diffusion term is added to the conservation laws of fluid dynamics

$$\frac{\partial}{\partial t}\rho = -\nabla\cdot(\rho \mathbf{V})$$

$$\frac{\partial}{\partial t}(\rho \mathbf{V}) = -\nabla\cdot(\rho \mathbf{V}\mathbf{V} + p\mathbf{I}) + \mathbf{J}\times\mathbf{B} + \nabla\cdot(\mu\nabla\mathbf{V})$$

$$\frac{\partial}{\partial t}\left(\frac{p}{\gamma-1}\right) = -\nabla\cdot\left(\frac{p}{\gamma-1}\mathbf{V}\right) - p\nabla\cdot\mathbf{V} + \nabla\cdot(\kappa_{\parallel}\nabla_{\parallel}T)$$

$$\frac{\partial}{\partial t}\mathbf{B} = -\nabla\times\mathbf{E} \qquad \mathbf{J} = \nabla\times\mathbf{B}$$

$$\mathbf{E} = -\mathbf{V}\times\mathbf{B} + \eta\mathbf{J} \qquad T = p/\rho$$

Differential operators at the centroid is discretized by the cell-centered finite-volume method

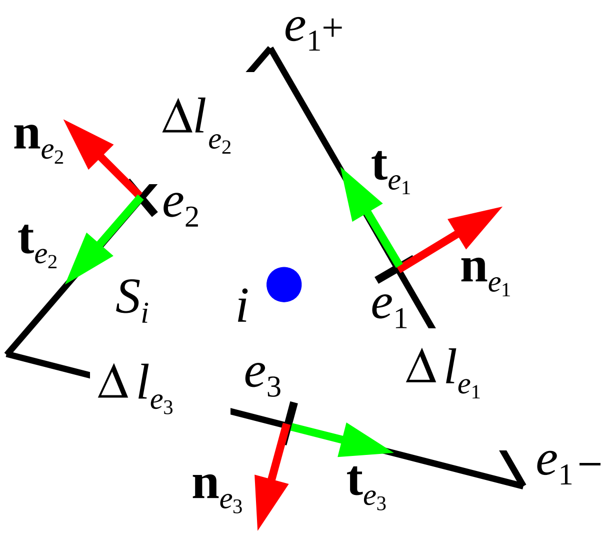

- Scalar and vector functions are discretized by a spectral method in the toroidal direction, φ
- .
$$f(R,\varphi,z) = \sum \widetilde{f}(R,z)e^{\Im n\varphi}$$
$$\mathbf{A}(R,\varphi,z) = \sum \widetilde{\mathbf{A}}(R,z)e^{\Im n\varphi}$$
- Poloidal plane is composed of the triangular (or quadrilateral) elements

- Following the cell-centered finite volume method, normal component and toroidal component of the vector function are defined at the triangular edges and the cell centroid, respectively.

- Discretization formulae for the divergence of a vector function **A** is described by

$$\left(\widetilde{\nabla\cdot\mathbf{A}}\right)_i \simeq \frac{1}{R_i S_i}\sum_e R_e \mathbf{n}_e\cdot\widetilde{\mathbf{A}}_e \Delta l_e + \frac{\Im n}{R_i}\mathbf{e}_\varphi\cdot\widetilde{\mathbf{A}}_i \quad .$$

Differential operators at the centroid is discretized by the cell-centered finite-volume method

Following above manner, the divergence of a tensor, the gradient of a scalar and of a vector at the cell centroid are obtained as follows.

$$\left(\nabla\cdot\widetilde{\mathbf{T}}\right)_i \simeq \frac{1}{R_i S_i}\sum_e R_e \mathbf{n}_e\cdot\widetilde{\mathbf{T}}_e \Delta l_e + \frac{\Im n}{R_i}\mathbf{e}_\varphi\cdot\widetilde{\mathbf{T}}_i + \frac{1}{R_i}\mathbf{e}_z\times\left(\mathbf{e}_\varphi\cdot\widetilde{\mathbf{T}}_i\right)$$

$$\left(\nabla\widetilde{f}\right)_i \simeq \frac{1}{R_i S_i}\sum_e R_e \widetilde{f}_e \mathbf{n}_e \Delta l_e + \frac{\Im n}{R_i}\widetilde{f}_i \mathbf{e}_\varphi - \frac{1}{R_i}\widetilde{f}_i \mathbf{e}_R$$

$$\begin{aligned}
\left(\nabla\widetilde{\mathbf{A}}\right)_i &\simeq \frac{1}{R_i S_i}\iint\left\{\mathbf{e}_R\mathbf{e}_k R\frac{\partial}{\partial R}\left(\widetilde{\mathbf{A}}\cdot\mathbf{e}_k\right) + \mathbf{e}_z\mathbf{e}_k R\frac{\partial}{\partial z}\left(\widetilde{\mathbf{A}}\cdot\mathbf{e}_k\right)\right\}dS \\
&\qquad + \frac{\Im n}{R_i}\mathbf{e}_\varphi\mathbf{e}_k\left(\widetilde{\mathbf{A}}\cdot\mathbf{e}_k\right) + \frac{1}{R_i}\mathbf{e}_\varphi\left(\mathbf{e}_z\times\widetilde{\mathbf{A}}_k\right) \\
&= \frac{1}{R_i S_i}\oint \mathbf{n}\,\mathbf{e}_k\left(R\widetilde{\mathbf{A}}\cdot\mathbf{e}_k\right)dl - \frac{1}{R_i S_i}\iint\left\{\mathbf{e}_R\mathbf{e}_k\left(\widetilde{\mathbf{A}}\cdot\mathbf{e}_k\right)\right\}dS \\
&\qquad + \frac{\Im n}{R_i}\mathbf{e}_\varphi\mathbf{e}_k\left(\widetilde{\mathbf{A}}\cdot\mathbf{e}_k\right) + \frac{1}{R_i}\mathbf{e}_\varphi\left(\mathbf{e}_z\times\widetilde{\mathbf{A}}_k\right) \\
&= \frac{1}{R_i S_i}\sum_e R_e \mathbf{n}_e \widetilde{\mathbf{A}}_e \Delta l_e - \frac{1}{R_i}\mathbf{e}_R\widetilde{\mathbf{A}}_i + \frac{\Im n}{R_i}\mathbf{e}_\varphi\widetilde{\mathbf{A}}_i + \frac{1}{R_i}\mathbf{e}_\varphi\left(\mathbf{e}_z\times\widetilde{\mathbf{A}}_i\right) \quad .
\end{aligned}$$

Another discretization is introduced only for the rotation operator

Surface integral is introduced instead of volume integral.

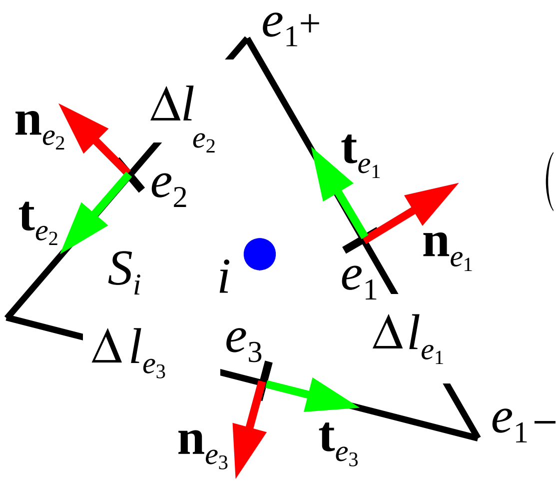

$$(\nabla\times\widetilde{\mathbf{A}})_i\cdot\mathbf{e}_\varphi \simeq \frac{1}{S_i}\iint\left(\frac{\partial\widetilde{A}_R}{\partial z}-\frac{\partial\widetilde{A}_z}{\partial R}\right)dS = -\frac{1}{S_i}\sum_e \mathbf{A}_e\cdot\widetilde{\mathbf{t}}_e\Delta l_e$$

$$(\nabla\times\widetilde{\mathbf{A}})_e\cdot\mathbf{n}_e \simeq \frac{1}{S_n}\iint\left\{n_R\left(\frac{1}{R}\frac{\partial\widetilde{A}_z}{\partial\varphi}-\frac{\partial\widetilde{A}_\varphi}{\partial z}\right)+n_z\left(\frac{1}{R}\frac{\partial\left(R\widetilde{A}_\varphi\right)}{\partial R}-\frac{1}{R}\frac{\partial\widetilde{A}_R}{\partial\varphi}\right)\right\}dS$$

$$= \frac{\Im n}{R_e}\widetilde{\mathbf{A}}_e\cdot\mathbf{t}_e-\frac{\left(R\widetilde{A}_\varphi\right)_{e+}-\left(R\widetilde{A}_\varphi\right)_{e-}}{R_e\Delta l_e}$$

$$(\widetilde{\nabla\times}\mathbf{A})_e\cdot\mathbf{t}_e \simeq \frac{1}{S_t}\iint\left\{t_R\left(\frac{1}{R}\frac{\partial\widetilde{A}_z}{\partial\varphi}-\frac{\partial\widetilde{A}_\varphi}{\partial z}\right)+t_z\left(\frac{1}{R}\frac{\partial\left(R\widetilde{A}_\varphi\right)}{\partial R}-\frac{1}{R}\frac{\partial\widetilde{A}_R}{\partial\varphi}\right)\right\}dS$$

$$= -\frac{\Im n}{R_e}\widetilde{\mathbf{A}}_e\cdot\mathbf{n}_e+\frac{\left(R\widetilde{A}_\varphi\right)_{+\delta n_e}-\left(R\widetilde{A}_\varphi\right)_{-\delta n_e}}{2R_e\Delta l_e}$$

Here, the divergence free of the rotation is satisfied numerically!!

$$(\nabla\cdot\widetilde{\nabla}\times\mathbf{A})_i = \frac{1}{R_iS_i}\sum_e\left\{\Im n\widetilde{\mathbf{A}}_e\cdot\mathbf{t}_e\Delta l_e-\left(\left(R\widetilde{A}_\varphi\right)_{e+}-\left(R\widetilde{A}_\varphi\right)_{e-}\right)\right\}-\frac{\Im n}{R_iS_i}\sum_e\widetilde{\mathbf{A}}_e\cdot\mathbf{t}_e\Delta l_e = 0$$

Implementation of a semi-implicit method for the time integration is now underway

The fast part (F) of the full MHD operator (M) is treated implicitly.

(cf. Schnack 1987)

$$\frac{(\rho\mathbf{V})^{n+1}-(\rho\mathbf{V})^{n}}{\Delta t} = \mathbf{F}(\rho\mathbf{V})^{n+1}+(\mathbf{M}-\mathbf{F})(\rho\mathbf{V})^{n}$$

For an arbitrary semi-implicit operator G

$$(\mathbf{I}-\Delta t\,\mathbf{G})(\rho\mathbf{V})^{n+1} = \underbrace{(\mathbf{I}+\Delta t\,\mathbf{M})}_{\text{Explicit}}(\rho\mathbf{V})^{n} - \underbrace{\Delta t\,\mathbf{G}}_{\text{Semi-implicit operator}}(\rho\mathbf{V})^{n}$$

G is chosen in consideration of the linearized MHD wave equation.

$$\mathbf{G}_1(\mathbf{V}) = \Delta t\,\nabla\times\nabla\times(\mathbf{V}\times\mathbf{B}_0)\times\mathbf{B}_0$$

We use a Laplacian semi-implicit operator for simplicity.

$$\mathbf{G}_2(\rho\mathbf{V}) = \alpha\Delta t\,V_{A0}^2\,\nabla^2(\rho\mathbf{V}) \qquad V_{A0}=\frac{B_0}{\sqrt{\rho_0}}$$

Equilibrium code, mesh generation code and parallelization has been implemented

- TOKAMAK equilibrium code MEUDAS which solves Grad–Shafranov eq. is used.
- Delaunay triangulations are constructed by Sloan's fast algorithm (Sloan, 1987).
- MPI is used for parallelization.
- METIS (Karypis and Kumar, 1999) is used for partitioning meshes.

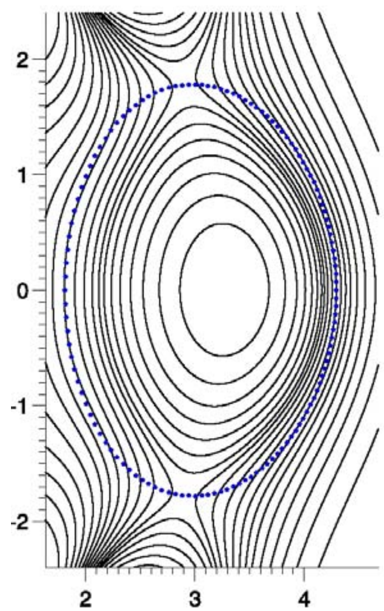

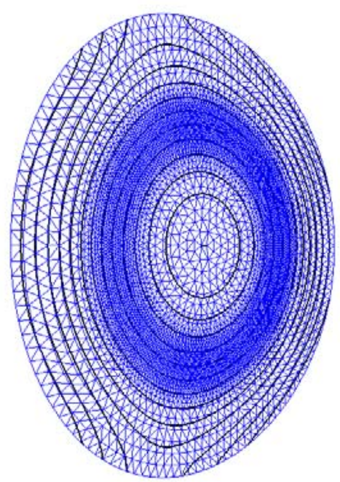

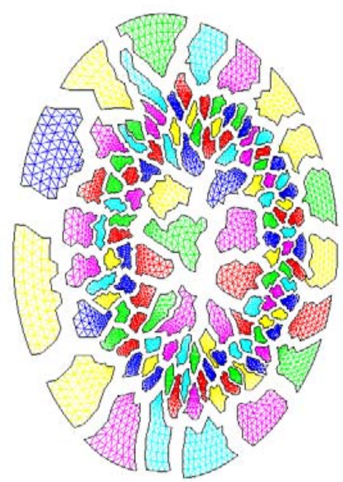

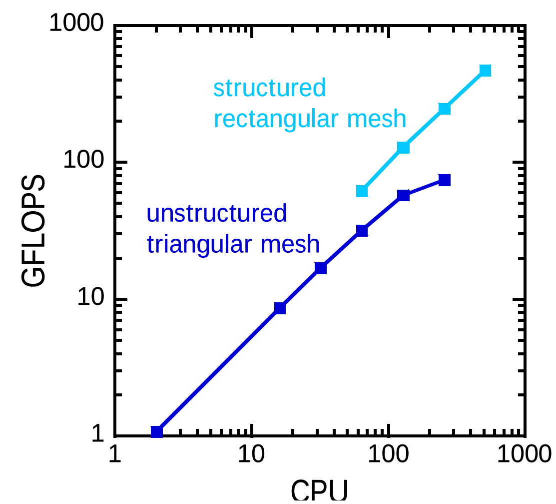

Nonlinear interactions among different scale MHD fluctuations are studied by MHFVSP code

- Previous works by Park (1995) or Nishimura (1999)

  High-n ballooning modes are excited by the equilibrium distortion and/or local pressure steepening due to the growth of the n=1 kink mode

- Viewpoint of this work

  Nonlinear evolution of high-n ballooning modes coexisting with a growing n=1 kink mode, and the role of interactions in the saturation mechanism

* As for this study, the vacuum region is not considered. The last closed flux surface is fixed at the perfect conducting boundary.

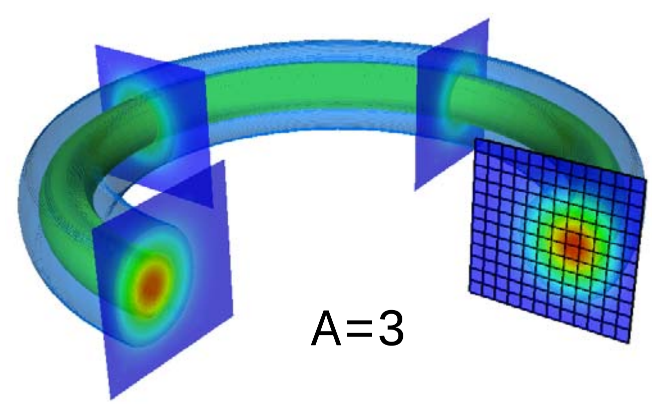

q and P profiles are chosen as kink and ballooning modes exist close to each other

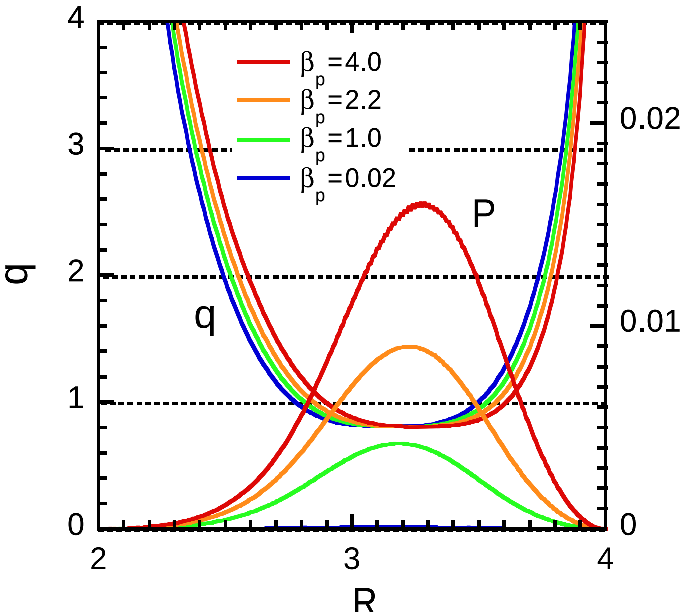

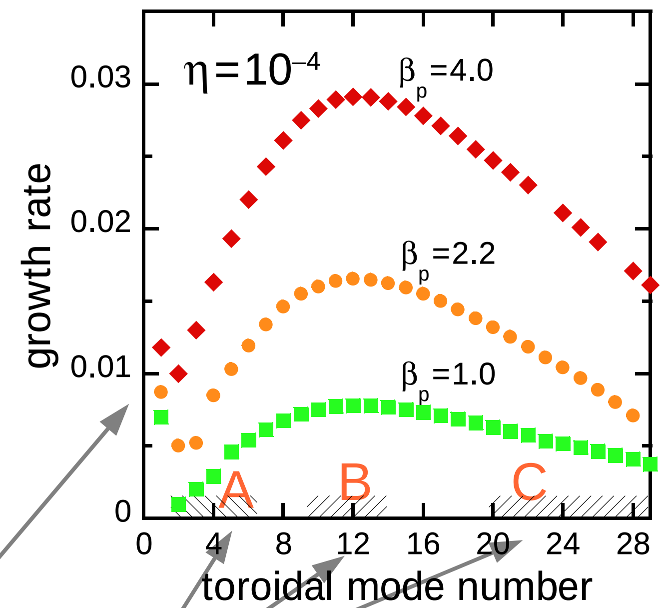

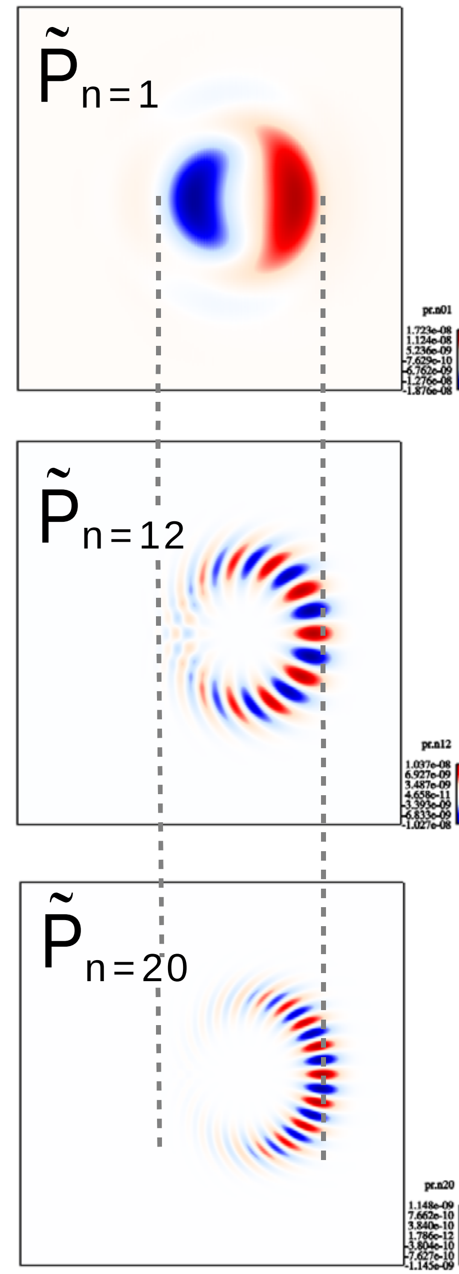

n=1 ： internal kink mode

Middle- and high- n ： ballooning modes

Classify into 3 groups by their growth rates

2 < n << 12	(group A)
n ~ 12 (most unstable)	(group B)
n >> 12	(group C)

Nonlinear simulations have been executed for β_p=1.0 case in which the growth rate of n=1 mode and that of modes of group B are about comparable.

Nonlinearly growing secondary modes form a helical structure

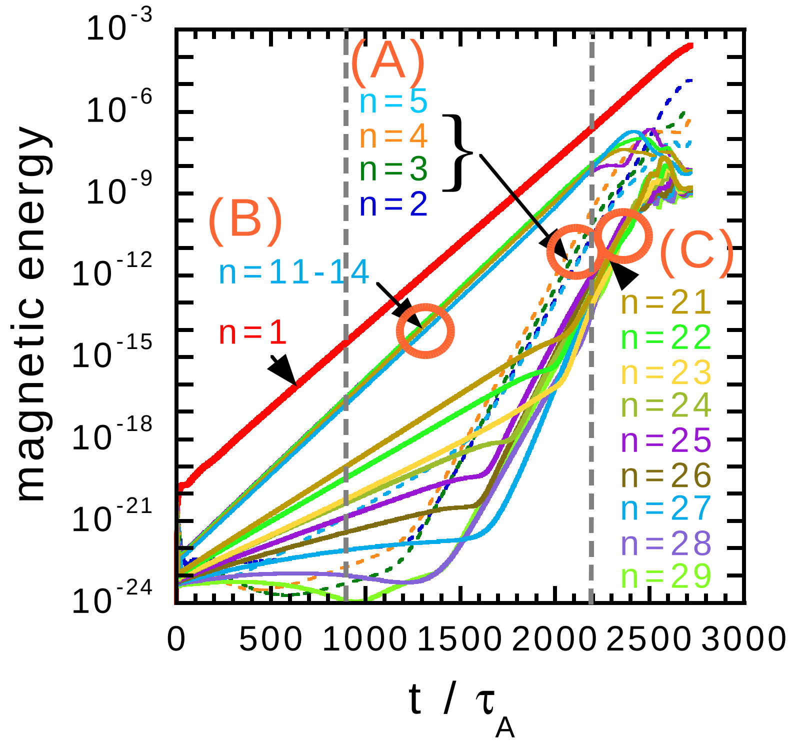

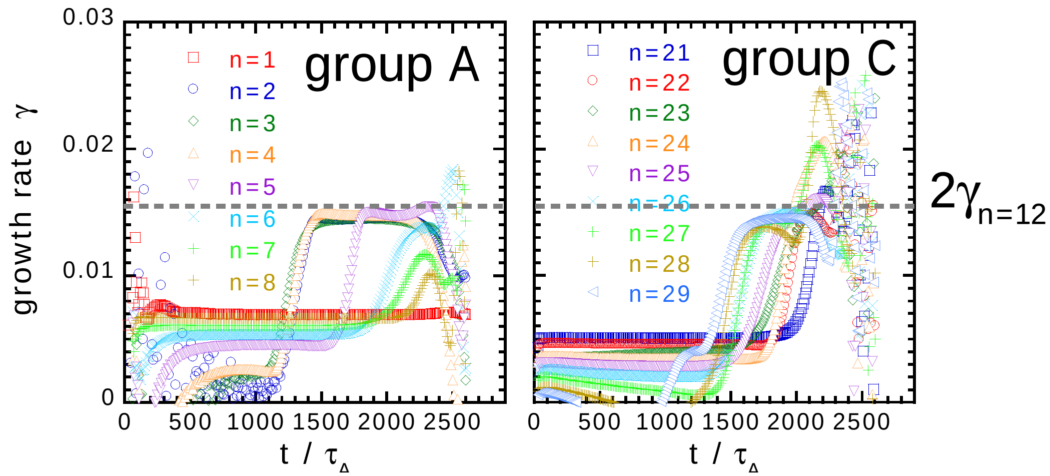

Modes of the group A and C are nonlinearly accelerated by those of the group B.

ex. n=12 and n=14 --► n=2 and n=26

Mode structure of n=21-29 (group C)

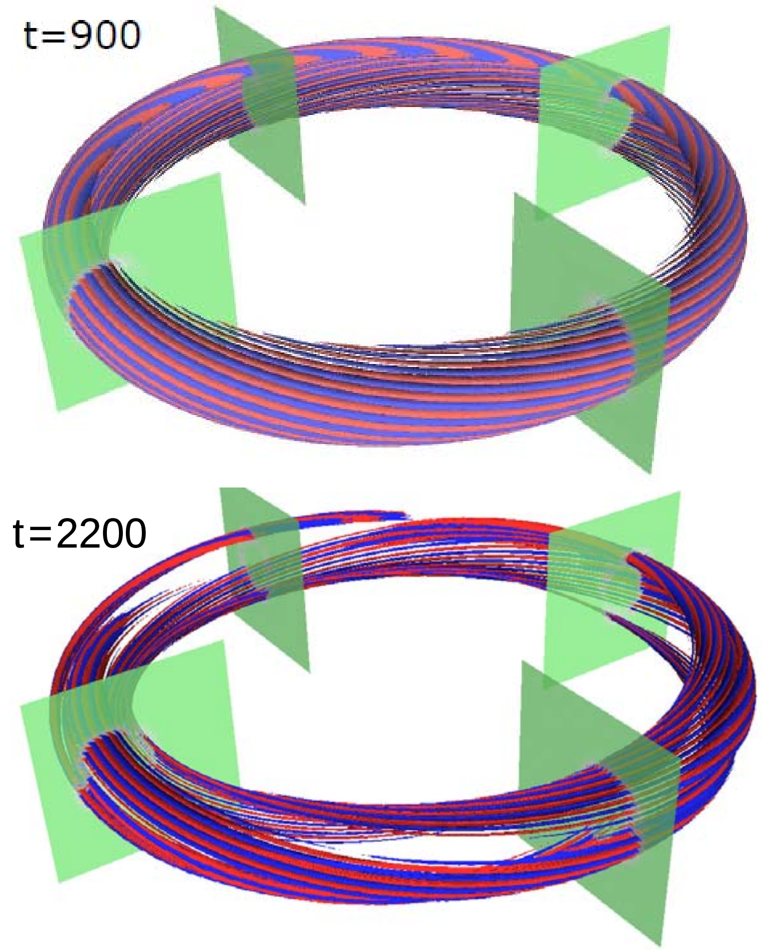

Nonlinearly growing secondary modes partially show a helically distorted structure, which suggests the phase of the ballooning modes aligns with that of the kink mode.

Ballooning fingers appears helically and then, they might seems to be saturated

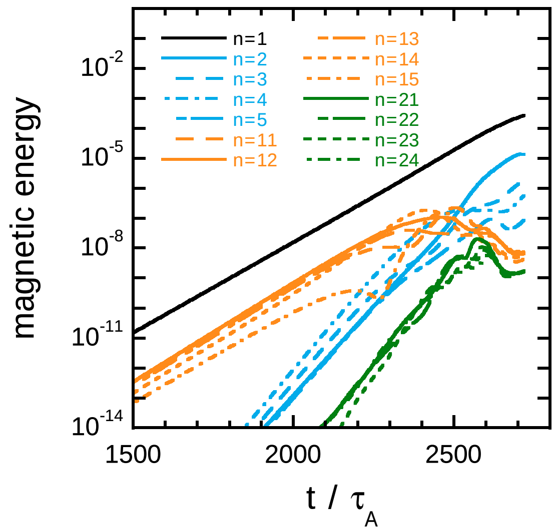

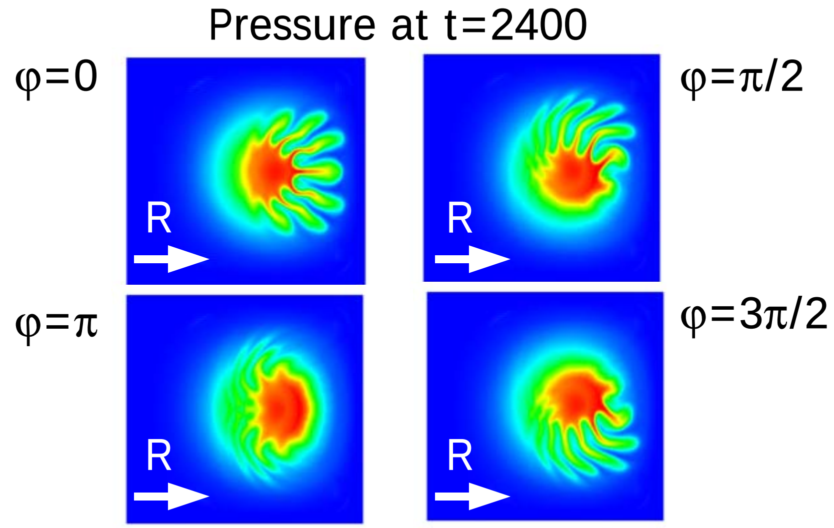

- Fluctuations of the ballooning modes might seem to be saturated, although the simulation has not been completed due to the numerical overshooting.
- The saturation might be caused by that fingers disappear in the bad-curvature region at $\varphi=\pi$ plane and appear in the good-curvature region where they are stable.
- In order to discuss the role of such a helical structure of ballooning modes in the saturation phenomena, the simulation needs to be advanced to the saturation process without numerical errors.
- Since the vacuum field might play an important role in energy transfer process, we are trying to implement a pseudo-vacuum model to improve the boundary condition.

Preliminary test has been done for a pseudo-vacuum model implemented code

- Replace the vacuum by low-dense and high-resistive plasma
- Preliminary test of the external kink mode in a cylindrical model case

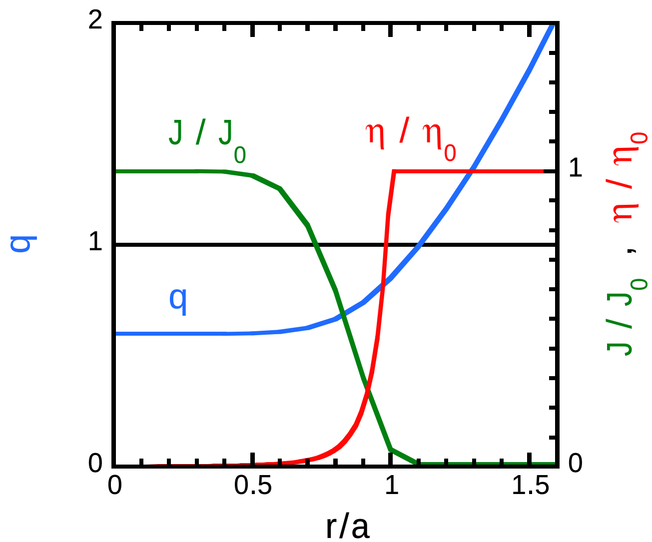

$$q_a = 0.85 \qquad \eta \propto T^{-3/2}$$

$$\eta_0 = 10^{-4} \;,\; \eta_v = 10^{-1}$$

$$\rho_0 = 1.0 \;,\; \rho_v = 0.1$$

P

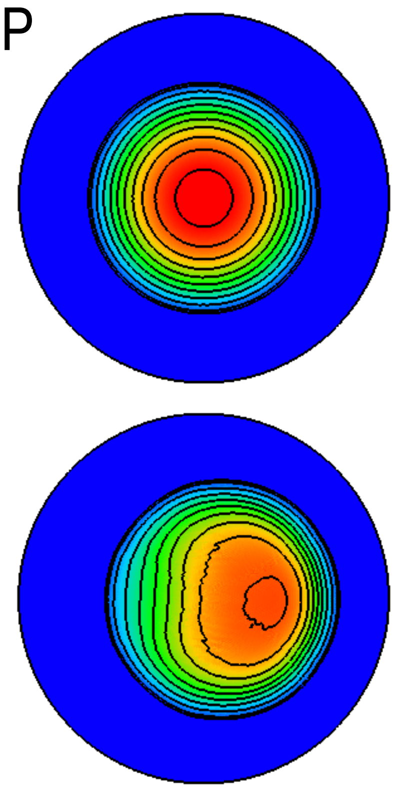

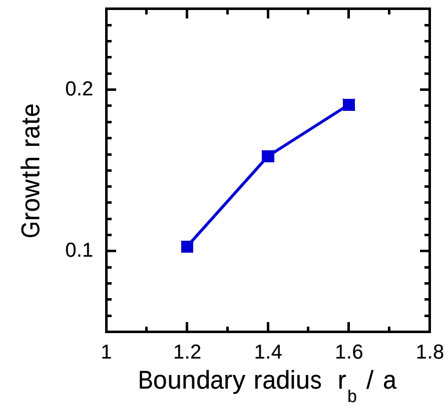

V

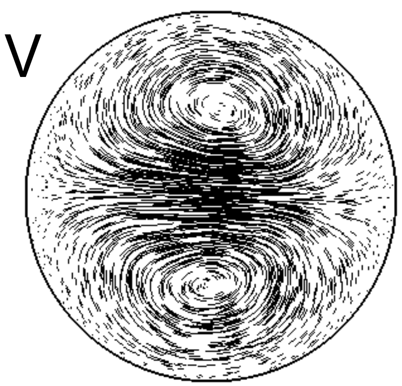

$\eta_v/\eta_0 = 10^3$ and $\rho_v/\rho_0 = 10^{-1}$ are confirmed to be available.

Larger η_v/η_0 and smaller ρ_v/ρ_0 are now being calculated.

Summary

- Recent progress of the development of a compressible full-MHD code based on the finite-volume method, MHFVSP code, is presented.
  - Discretization formulae of differential operators satisfying the divergence free condition of the magnetic field are shown .
  - Equilibrium code, mesh generation code, parallelization and pseudo-vacuum model has been implemented.
- Evolution of high-n ballooning modes interacting with a low-n kink mode is investigated.
  - The coupling among linear ballooning modes generates nonlinearly growing secondary modes which exhibit the helically distorted ballooning structure due to the interactions with the n=1 kink mode.
  - Since the helically distorted ballooning structure is not localized in the bad-curvature region, it might play a role in the reduction of the growth of the modes or the saturation, although further investigations are required to clear the detailed mechanism.